

## 2 – 3 $\mu\text{m}$ mid infrared light sources using InGaAs/GaAsSb “W” type quantum wells on InP substrates

C. H. Pan, S. D. Lin, and C. P. Lee

Citation: [Journal of Applied Physics](#) **108**, 103105 (2010); doi: 10.1063/1.3506427

View online: <http://dx.doi.org/10.1063/1.3506427>

View Table of Contents: <http://scitation.aip.org/content/aip/journal/jap/108/10?ver=pdfcov>

Published by the [AIP Publishing](#)

---

### Articles you may be interested in

[InN/InGaN multiple quantum wells emitting at 1.5  \$\mu\text{m}\$  grown by molecular beam epitaxy](#)  
Appl. Phys. Lett. **98**, 061901 (2011); 10.1063/1.3552195

[Silicon emitter for shortwave infrared \( 1.6 – 3  \$\mu\text{m}\$  \) band by light down-conversion](#)  
Appl. Phys. Lett. **97**, 211104 (2010); 10.1063/1.3521277

[Planar silicon light emitting arrays for the 3 – 12  \$\mu\text{m}\$  spectral band](#)  
J. Appl. Phys. **106**, 113106 (2009); 10.1063/1.3264733

[Polarization-independent intersubband based GaInAsN quantum-well photodetector with dominant detection at 1.42  \$\mu\text{m}\$](#)   
Appl. Phys. Lett. **94**, 093503 (2009); 10.1063/1.3089868

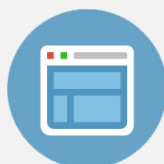
[Recombination processes in midinfrared InGaAsSb diode lasers emitting at 2.37  \$\mu\text{m}\$](#)   
Appl. Phys. Lett. **89**, 051104 (2006); 10.1063/1.2243973

---



## Re-register for Table of Content Alerts

Create a profile.



Sign up today!



## 2–3 $\mu\text{m}$ mid infrared light sources using InGaAs/GaAsSb “W” type quantum wells on InP substrates

C. H. Pan,<sup>a)</sup> S. D. Lin, and C. P. Lee

*Department of Electronics Engineering, National Chiao Tung University, Hsinchu 300, Taiwan*

(Received 14 July 2010; accepted 23 September 2010; published online 18 November 2010)

We have investigated the InGaAs/GaAsSb/InAlGaAs/InAlAs type-II “W” quantum wells (QWs) grown on InP substrates by molecular beam epitaxy. The photoluminescence (PL) emission wavelength longer than 2.56  $\mu\text{m}$  at room temperature (RT) is demonstrated for the first time in this material system. The PL emission peaks of our designed samples can cover a wide range from 2 to 2.5  $\mu\text{m}$  at cryogenic temperature. The samples show good optical quality that the reduction in integrated PL intensity is only around one order of magnitude from 35 K to RT. We found that the integrated PL intensity decreased as the emission wavelength increased, which is due to the reduction in the electron-hole wave function overlap. This is consistent with the calculated result. In the power dependent PL measurements, the emission peak of “W” type QWs show blue shifts with the excitation power ( $P_{\text{ex}}$ ) but does not follow the  $P_{\text{ex}}^{1/3}$  rule as predicted by type-II band bending model. The localized states filling effect gives reasonable explanations for the observed phenomena. © 2010 American Institute of Physics. [doi:10.1063/1.3506427]

### I. INTRODUCTION

Mid-infrared (mid-IR) light source are useful in many different applications, such as environment monitoring, industrial gas detection, life science, and military security, etc.<sup>1,2</sup> In semiconductors, the mid-IR lasers with wavelengths in the 2–3  $\mu\text{m}$  range have been fabricated on GaSb substrates using InGaAsSb/AlGaAsSb type-I quantum wells (QWs).<sup>3,4</sup> It is, however, much more desirable to use a more popular substrate such as InP, which is cheaper, has a better quality and has a better thermal conductivity. But to grow type-I QWs with emission wavelength longer than 2  $\mu\text{m}$  on InP is difficult due to lattice mismatch.<sup>5</sup> The longest wavelength reported is 2.33  $\mu\text{m}$  with a highly strained InAs/InGaAs system.<sup>6–8</sup> However, if we use the type-II InGaAs/GaAsSb heterostructure on InP substrates, we can bypass the requirement for small band gap materials by using the staggered band alignment and the wavelength can be extended longer without being limited by the band gap of the constituent materials. In this work, the mid-IR light sources between 2–3  $\mu\text{m}$  were studied using the type-II “W” type QWs.<sup>9–11</sup> We demonstrate that the emission wavelength can be extended longer than 2.56  $\mu\text{m}$  at room temperature.

### II. EXPERIMENTS

The structure of a “W” type QW used in this work is composed of symmetric InGaAs/GaAsSb/InGaAs layers, which are sandwiched between two InAlAs barrier layers, lattice matched to InP. The barrier layers provide a strong quantum confinement to enhance the electron-hole wave function overlap and hence the optical matrix element. The band alignment of a represented  $\text{In}_{0.53}\text{Ga}_{0.47}\text{As}$  (lattice-matched to InP)/ $\text{GaAs}_{0.4}\text{Sb}_{0.6}$  ( $\sim 0.7\%$  compressive strain)/ $\text{In}_{0.52}\text{Al}_{0.48}\text{As}$  “W” structure is shown in Fig. 1(a). In

order to optimize the structure, we first calculated the emission wavelength and the amount of electron-hole wavelength overlap by solving the Schrodinger equation using the effective mass approximation with the parameters taken from the previous articles.<sup>12–14</sup> Figs. 1(b) and 1(c), respectively, show the layer thickness dependence of the “W” type QWs emission wavelength and the electron-hole wave function overlap. Basically, wavelength can be tuned in the range from 1.8 to 3  $\mu\text{m}$  via modifying the thickness of InGaAs and GaAsSb. However, the wave function overlap decreases when the emission wavelength is increased, as indicating in Fig. 1(c). This is an intrinsic feature for the “W” type QW. The electron and hole are confined separately in different layers, the electron in the two coupled InGaAs layers and the hole in the GaAsSb layer, as shown in Fig. 1(a). Since the confinement potentials are large ( $>0.4$  eV) for both carriers, the quantization energies are decided by their own layer thickness; a thicker InGaAs or GaAsSb layer leads to a smaller electron or hole quantization energy and hence a longer emission wavelength. Although the increase of the InGaAs or GaAsSb layer thickness extends the emission wavelength, it also makes the electron and hole wave functions more concentrated in individual layers, and causes the reduction in electron-hole overlap. Obviously, it is a trade-off between the long wavelength emission and the optical matrix element.<sup>11</sup> Although the wavelength can be extended with more Sb content in GaAsSb, the raised conduction band edge, however, blocks the electron wave function penetration into the GaAsSb layer causing a reduction in the electron-hole wave function overlap. So it is still a trade-off situation. Since the optical matrix element is an important parameter for optoelectronic devices, structure optimization of the “W” type QWs is very important.

Our samples were grown on S-doped (001) InP substrates by a Veeco GEN II solid-source molecular beam epitaxy system. The  $\text{As}_2$  and  $\text{Sb}_2$  species were used through the

<sup>a)</sup>Electronic mail: panjoan.ee95g@nctu.edu.tw.

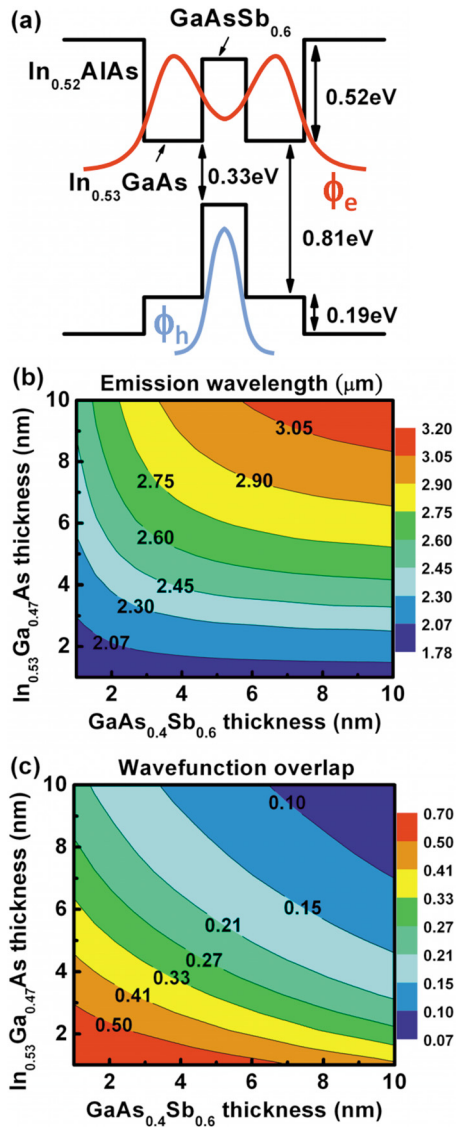


FIG. 1. (Color online) (a) Energy band diagram of the “W” type QW with the wave functions for electron and hole. Calculated contour plots of (b) emission wavelength and (c) electron-hole wave function overlap vs InGaAs (vertical axis) and GaAsSb (horizontal axis) layer thickness.

equipped needle-valve controlled cracking cells. The wafer surface temperature was monitored by an infrared pyrometer. For the multilayer growth consideration, the structure of the “W” QWs designed here are the symmetric  $\text{In}_{0.53}\text{Ga}_{0.47}\text{As}/\text{GaAsSb}/\text{In}_{0.53}\text{Ga}_{0.47}\text{As}$  layers sandwiched between two 2 nm  $\text{In}_{0.36}\text{Al}_{0.32}\text{Ga}_{0.32}\text{As}$  tensile strain layers to compensate the compressive strain in the GaAsSb layer. Nine such “W” type QWs spaced by 25 nm  $\text{In}_{0.52}\text{Al}_{0.48}\text{As}$  barrier layers were grown and placed between two 200 nm  $\text{In}_{0.52}\text{Al}_{0.48}\text{As}$  layers, as shown in Fig. 2. In order to optimize the “W” structure, this study was performed systematically by varying the thickness of the InGaAs/GaAsSb layers, the composition of the GaAsSb layer and the growth temperature. The growth parameters are listed in Table I, where three series of samples are grouped and labeled as A, B, and C. Groups A and B are samples with variable thicknesses of InGaAs and GaAsSb, respectively. Group C contains samples with different Sb mole fraction in the GaAsSb layer

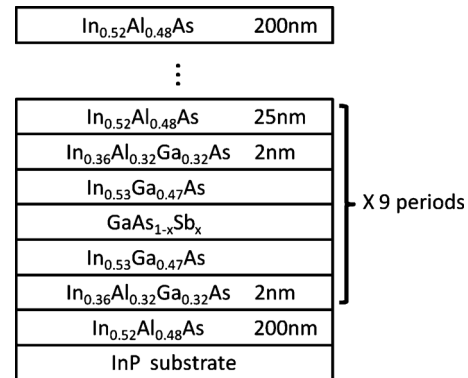


FIG. 2. The structure of the designed “W” type QWs.

by adjusting the  $\text{Sb}_2/\text{As}_2$  beam equivalent pressure (BEP) ratio. The growth temperature is also changed from group A to group C.

### III. RESULTS AND DISCUSSION

After the samples were grown, the photoluminescence (PL) measurement was carried out using a 488 nm  $\text{Ar}^+$  laser as the excitation source and a thermal electric cooled InGaAs(Sb) detector. All the PL spectra were calibrated by the response spectrum of a 1000 °C black radiation source. The PL spectra measured at 20 K are presented in Fig. 3(a). The peak emission wavelength ( $\lambda_{\text{peak}}$ ) covers the range from  $\sim 2$  to  $\sim 2.5$   $\mu\text{m}$ . As summarized in Table I, the  $\lambda_{\text{peak}}$  can be extended from 2.05 to 2.47  $\mu\text{m}$  by increasing the InGaAs layer thickness from 4 to 10 nm as shown in group A, and can be extended from 2.17 to 2.42  $\mu\text{m}$  with the increase of GaAsSb layer thickness from 2 to 4 nm (in group B). The sensitivity of  $\lambda_{\text{peak}}$  to the InGaAs/GaAsSb layer thicknesses agrees well with our calculations. Notice that the full width of half to maximum (FWHM) of the PL spectra increases from 13.9 to 22.7 meV when the GaAsSb layer thickness is reduced, as indicated in group B. This is caused by the energy level broadening due to the thickness fluctuation when the GaAsSb layer is thin. The  $\lambda_{\text{peak}}$  can be also extended by the increase of the Sb-content, as shown by group C samples. The Sb fraction is determined by fitting the  $\lambda_{\text{peak}}$  with the calculation results. The  $\lambda_{\text{peak}}$  goes from 2.37 to 2.48  $\mu\text{m}$ , around a 23 meV difference, as the Sb mole fraction increases from 0.74 to 0.78. We can also see the effect of growth temperature by comparing these three groups of samples. It is found that the samples grown at a lower temperature have a longer emission wavelength and a narrower PL spectrum. This may indicate that the Sb incorporation is more efficient and the fluctuation of alloy composition is less at lower growth temperatures.<sup>15,16</sup> Figure 3(b) shows the integrated PL intensity as a function of the emission wavelength. It clearly shows the trade-off situation as predicted by the simulation. The calculated curve, which is based on the assumption that the integrated PL intensity is proportional to the square of the wave function overlap, fits very nicely with the experimental results.

The optical transition of the type-II heterostructure has been extensively studied previously.<sup>17,18</sup> The  $\lambda_{\text{peak}}$  usually blue shifts with the excitation power ( $P_{\text{ex}}$ ), and the amount of

TABLE I. The InGaAs/GaAsSb layer thickness, the  $\text{Sb}_2/\text{As}_2$  BEP ratio, the summarized PL peak wavelength, and FWHM of the “W” type QW samples in group A, B, and C.

Sample number	Layer thickness (nm)			BEP ratio $\text{Sb}_2/\text{As}_2$	Growth T(°C)	$\lambda_{\text{peak}}$ ( $\mu\text{m}$ )	FWHM (meV)
	$\text{In}_{0.53}\text{GaAs}$ (lattice match)	$\text{GaAs}_{1-x}\text{Sb}_x$	X				
A1	4	3	0.58	1.8	475	2.05	24.7
A2	7	3	0.58	1.8	475	2.34	22.4
A3	10	3	0.58	1.8	475	2.47	25.4
B1	5	2	0.65	2.0	470	2.17	22.7
B2	5	3	0.65	2.0	470	2.27	18.8
B3	5	4	0.65	2.0	470	2.42	13.9
C1	4	3	0.74	1.8	460	2.37	12.6
C2	4	3	0.78	2.9	460	2.48	13.8

shift is linearly dependent on the one-third power of  $P_{\text{ex}}$  because of the band bending effect caused by the accumulation of spatially separated electrons and holes in the adjacent triangular interface potential wells. However, the power dependent emission of a “W” type QW has never been studied in detail. We found that, although  $\lambda_{\text{peak}}$  shifts to a shorter wavelength as  $P_{\text{ex}}$  is increased, the energy shift does not obey the  $P_{\text{ex}}^{1/3}$  law, especially under low  $P_{\text{ex}}$ . The power dependent spectra of sample A1 and C1 are presented in Fig. 4(a), and the amount of energy shift is plotted as a function of the  $P_{\text{ex}}$  in Fig. 4(b) along with the ideal  $P_{\text{ex}}^{1/3}$  curve for comparison

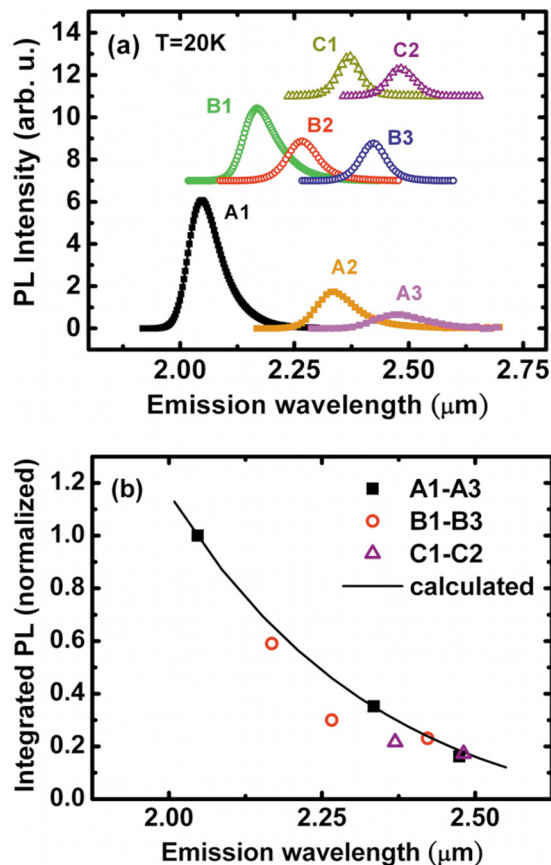


FIG. 3. (Color online) (a) PL spectra of samples in group A, B, C, and (b) integrated PL intensity (normalized at sample A1) plotted against the peak wavelength. The calculated result is plotted as the solid curve.

(both axes in log scale). Since the curves are not linear in this log-log plot, the energy shift vs.  $P_{\text{ex}}$  does not follow any power law. We also notice that sample A1 has a more pronounced energy shift than sample C1. This power dependent behavior is not due to the heating effect since the integrated PL intensity is linearly proportional to  $P_{\text{ex}}$ , as shown in the inset of Fig. 4(b). The possible reason for the amount of blue shift to deviate from the  $P_{\text{ex}}^{1/3}$  law is the state filling effect of the localized states. The localized states are caused by interface roughness and alloy composition fluctuation, which are common in the ternary alloy.<sup>19,20</sup> Under low excitation powers, the generated carriers occupy the localized states with lower energies. As the amount of carriers is increased with increased  $P_{\text{ex}}$ , higher energy states are occupied and therefore the peak of the emitted light shifts to a shorter wavelength. The extended tail in the low energy side of the PL

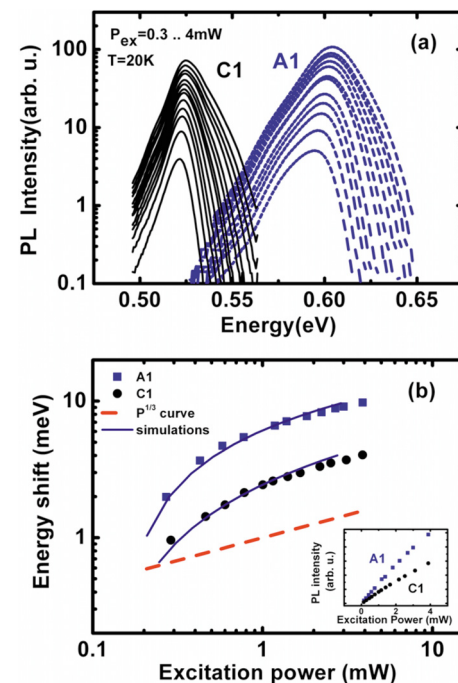


FIG. 4. (Color online) (a) Power dependence PL spectra of sample A1 and sample C1, and (b) the energy shifts vs  $P_{\text{ex}}$  along with the simulation results and the ideal  $P_{\text{ex}}^{1/3}$  curve for comparison. The inset shows the power dependence of the integrated PL intensity.

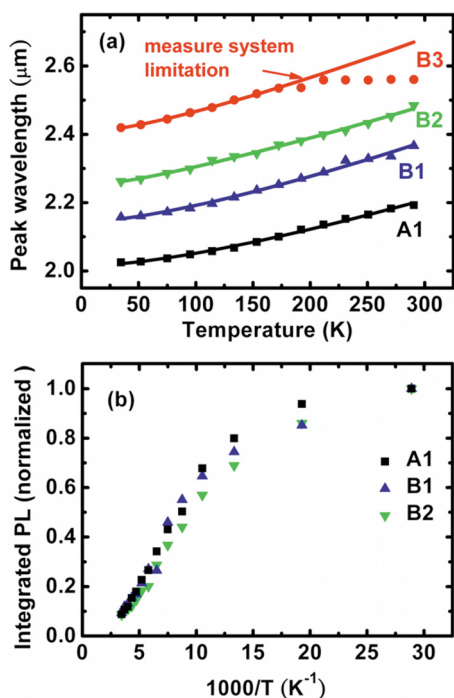


FIG. 5. (Color online) (a) PL peak wavelength vs temperature in sample A1, B1, B2, and B3. (b) Temperature dependence of the normalized integrated PL intensity (points) with the fitted Varshni curves.

spectra shown in Figs. 3(a) and 4(a) is an indication of the radiation from these localized states. We have performed a simulation for such effect by assuming a joint density of states associated with the localized states as  $\text{erfc}[(\langle E_0 \rangle - E)/\delta E]$ , where  $\text{erfc}$  is the complementary error function,  $\langle E_0 \rangle$  and  $\delta E$  refer to the average and the standard deviation of the transition energy to take into account of the inhomogeneous broadening effect.<sup>21</sup>  $\delta E$  values of 30 and 18 meV were used in the calculation for samples A1 and C1. When the Fermi level is raised because of a higher pumping power, the emission peak blue shifts to a higher energy. The calculated results are shown together with the experiment data in Fig. 4(b). Excellent agreement between the calculated and the experimental results was achieved. Since sample A1 has a broader PL spectrum, it has a larger  $\delta E$  and a more pronounced states filling effect. Therefore it has a larger energy shift compared to that of sample C1. In general, both the states filling effect and the band bending effect should contribute to the energy shift. The reason that states filling effect dominates here is due to the large  $\delta E$  and the relative small band bending effect in “W” type QWs.

In order to examine the sample emission at higher temperatures, we have done the PL measurement with the temperature varied from 35 to 290 K under a fixed 10 mW excitation power. Figure 5(a) shows  $\lambda_{\text{peak}}$  as a function of temperature for samples A1, B1, B2, and B3. As the temperature raises, the emission wavelength red shifts as expected due to the band gap shrinkage. The cut-off  $\lambda_{\text{peak}}$  around 2.56  $\mu\text{m}$  in the spectrum of sample B3 is caused by the lens absorption in our measure system. The temperature dependence of the emission peak is fitted well with the Varshni relation,  $E(T) = E(0) - \alpha T^2 / (\beta + T)$ , as shown the curves in Fig. 5(a). The peak wavelength can be extrapolated

to 2.67  $\mu\text{m}$  at room temperature in sample B3. The temperature dependence of the normalized integrated PL intensity is presented in Fig. 5(b). It shows only about one order of magnitude reduction in the PL intensity from LT to RT. The reason that the “W” type QWs emission intensity can be well sustained to high temperatures is due to the good carrier confinement and a low density of nonradiative defects in our samples.

#### IV. CONCLUSIONS

In conclusion, we have studied the InGaAs/GaAsSb/InAlGaAs/InAlAs “W” type QWs grown on InP substrates. The emission wavelength covers the range from  $\sim 2$  to  $\sim 2.5$   $\mu\text{m}$  at low temperature. The trade-off between long wavelength emission and high optical matrix element predicted by the simulation has been confirmed by the results of PL spectra. The type-II band alignment in the “W” structure has been characterized by the power dependent PL measurements. The peak position shifts to shorter wavelength as  $P_{\text{ex}}$  increases. It was found the amount of energy shifts does not follow the  $P_{\text{ex}}^{1/3}$  law as most type II structures. The localized states filling effect due to the surface roughness and alloy fluctuation is proposed to explain the observed phenomenon. The calculated results agree well with the experiment results. The temperature dependent PL spectra show the well sustained emission at RT, and the emission wavelength of the “W” type QWs can be extended to over 2.56  $\mu\text{m}$ . According to our experiments and simulation results, it is very promising to develop the Mid-IR lasers on InP substrates employing the “W” structure of InGaAs/GaAsSb/InGaAs QWs.

#### ACKNOWLEDGMENTS

We acknowledge the support from the National Science Council under Contract Nos. NSC96-2221-E-009-211-MY3 and NSC98-2120-M-009-002, Center for Nano Science and Technology of National Chiao Tung University, National Nano Device Laboratories, and “Aim for the Top University Plan” of the National Chiao Tung University and Ministry of Education, Taiwan, R.O.C.

<sup>1</sup>U. Willer, M. Saraji, A. Khorsandi, P. Geiser, and W. Schade, *Opt. Lasers Eng.* **44**, 699 (2006).

<sup>2</sup>A. Godard, *C. R. Phys.* **8**, 1100 (2007).

<sup>3</sup>W. Li, J. B. Héroux, H. Shao, and W. I. Wang, *Appl. Phys. Lett.* **84**, 2016 (2004).

<sup>4</sup>J. A. Gupta, P. J. Barrios, J. Lapointe, G. C. Aers, and C. Storey, *Appl. Phys. Lett.* **95**, 041104 (2009).

<sup>5</sup>G. K. Kuang, G. Bohm, M. Grau, G. Rosel, R. Meyer, and M.-C. Amann, *Appl. Phys. Lett.* **77**, 1091 (2000).

<sup>6</sup>T. Sato, M. Mitsuhashi, N. Nunoya, T. Fujisawa, F. Kano, and Y. Kondo, *IEEE Photon. Technol. Lett.* **20**, 1045 (2008).

<sup>7</sup>D. G. Revin, J. W. Cockburn, M. J. Steer, R. J. Airey, M. Hopkinson, A. B. Krysa, L. R. Wilson, and S. Menzel, *Appl. Phys. Lett.* **90**, 021108 (2007).

<sup>8</sup>S. Y. Zhang, D. G. Revin, J. W. Cockburn, K. Kennedy, A. B. Krysa, and M. Hopkinson, *Appl. Phys. Lett.* **94**, 031106 (2009).

<sup>9</sup>J. Y. T. Huang, L. J. Mawst, T. F. Kuech, X. Song, S. E. Babcock, C. S. Kim, I. Vurgaftman, J. R. Meyer, and A. L. Holmes, *J. Phys. D* **42**, 025108 (2009).

<sup>10</sup>L. J. Mawst, J. Y.-T. Huang, D. P. Xu, J.-Y. Yeh, G. Tsvit, T. F. Kuech, and N. Tansu, *IEEE J. Sel. Top. Quantum Electron.* **14**, 979 (2008).

<sup>11</sup>J. Y. T. Huang, D. P. Xu, L. J. Mawst, T. F. Kuech, I. Vurgaftman, and J. R. Meyer, *IEEE J. Sel. Top. Quantum Electron.* **13**, 1605 (2007).

- <sup>12</sup>J. Hu, X. G. Xu, J. A. H. Stotz, S. P. Watkins, A. E. Curzon, M. L. W. Thewalt, N. Matine, and C. R. Bolognesi, *Appl. Phys. Lett.* **73**, 2799 (1998).
- <sup>13</sup>C. Pryor and M.-E. Pistol, *Phys. Rev. B* **72**, 205311 (2005).
- <sup>14</sup>I. Vurgaftman, J. R. Meyer, and L. R. Ram-Mohan, *J. Appl. Phys.* **89**, 5815 (2001).
- <sup>15</sup>C. Renard, X. Marcadet, J. Massies, and O. Parillaud, *J. Cryst. Growth* **278**, 193 (2005).
- <sup>16</sup>J. F. Klem, O. Blum, S. R. Kurtz, I. J. Fritz, and K. D. Choquette, *J. Vac. Sci. Technol. B* **18**, 1605 (2000).
- <sup>17</sup>M. C. Lo, S. J. Huang, C. P. Lee, S. D. Lin, and S. T. Yen, *Appl. Phys. Lett.* **90**, 243102 (2007).
- <sup>18</sup>N. N. Ledentsov, J. Böhrer, M. Beer, F. Heinrichsdorff, M. Grundmann, D. Bimberg, S. V. Ivanov, B. Ya. Meltser, S. V. Shaposhnikov, I. N. Yassievich, and N. N. Faleev, P. S. Kop'ev, and Zh. I. Alferov, *Phys. Rev. B* **52**, 14058 (1995).
- <sup>19</sup>M. Dinu, J. E. Cunningham, F. Quochi, and J. Shah, *J. Appl. Phys.* **94**, 1506 (2003).
- <sup>20</sup>A. Ait-Ouali, R. Y.-F. Yip, J. L. Brebner, and R. A. Masut, *J. Appl. Phys.* **83**, 3153 (1998).
- <sup>21</sup>J. Christen and D. Bimberg, *Phys. Rev. B* **42**, 7213 (1990).